Pergamon

Int. J. Heat Mass Transfer. Vol. 41, Nos 4–5, pp. 745–756, 1998

Printed in Great Britain
0017–9310/98 $19.00+0.00

PII: S0017–9310(97)00158–0

Modelling of radiative heat transfer in enclosures with obstacles

P. J. COELHO, J. M. GONÇALVES and M. G. CARVALHO

Instituto Superior Técnico, Technical University of Lisbon, Mechanical Engineering Department, Av. Rovisco Pais, 1096 Lisboa Codex, Portugal

and

D. N. TRIVIC

Institute of Nuclear Sciences "Vinca", Laboratory of Thermal Engineering and Energy Research, P.O. Box 522, 11001 Belgrade, Yugoslavia

(*Received* 5 *March* 1997 *and in final form* 12 *May* 1997)

Abstract—Radiation models suitable for incorporation in reactive fluid flow codes are extended to calculate radiation in enclosures containing obstacles of very small thickness. The discrete transfer, the discrete ordinates and the finite volume method are employed to predict the heat transfer in two-dimensional enclosures and the results are compared with zone method calculations, with the total exchange areas determined by the Monte-Carlo method. All the methods predict similar heat fluxes, but the computational requirements are different. The discrete ordinates and the finite volume method are the most economical ones. An application to a utility boiler is also presented. © 1997 Elsevier Science Ltd.

1. INTRODUCTION

The development of radiative heat transfer models has received significant attention for many years and several models are presently available [1]. However, in many relevant engineering problems, radiation is not the only physical phenomenon involved. In particular, in combustion equipment the problem of calculation of radiative heat transfer is coupled with the modelling of a turbulent reactive flow. In this case successful models, such as the zone [2] and the Monte-Carlo [3] methods, are seldom used because the solution algorithm is rather different from the solution algorithm employed in the modelling of the reactive flow, and also because they are computationally demanding. Other models, such as the flux method of Schuster–Schwarzchild [4] and its generalization for two- and three-dimensional domains, have low accuracy. The spherical harmonics method is not accurate for low-order approximations, except in optically thick media, and the increase of accuracy achievable using high order approximations is mathematically involved [5]. Three of the most attractive methods, as far as accuracy and computational requirements are concerned, are the discrete transfer [6], the discrete ordinates [7, 8] and the finite-volume [9, 10] methods. They are easily incorporated in reactive fluid flow codes, and a comparison of their performance has recently been published [11].

A related problem of practical relevance which has received little attention in the literature is the radiative heat transfer in enclosures containing obstacles, such as protrusions and obstructions. This problem was addressed by Sànchez and Smith [12], who presented a study on surface radiation exchange for two-dimensional rectangular enclosures with protrusions and obstructions containing a transparent medium, using the discrete ordinates method. A similar method was applied to a three-dimensional furnace with internal cooling-pipes which behave as obstacles as far as radiation is concerned [13]. Attention was focused on modelling highly directional shadowing effects caused by the cooling-pipes in the radiation intensity field. A simple procedure to deal with irregular Cartesian-coordinates-based geometries, and suitable to treat protrusions, obstructions and curved or inclined surfaces was proposed by Chai *et al.* [14, 15]. This procedure was incorporated in the discrete ordinates method [14] and in the finite volume method [15], and applied to several two-dimensional problems.

In some applications, the thickness of the obstacles is very small. A typical example occurs in power station boilers, where panels of superheaters are often hanged from the top of the radiation chamber. The thickness of these panels is much smaller than the overall dimensions of the boiler, typically two or three orders of magnitude. Therefore, if they were modelled as obstacles of finite thickness, it would be necessary to use small control volumes in the direction normal to the superheaters, in their neighbourhood, in order to account for their presence. Moreover, the grid used in the radiation calculations must be compatible with the grid employed to solve the transport equations that describe the turbulent reactive flow. The best way

NOMENCLATURE

A area [m^2]
A_x, A_y area normal to the x- and y-directions, respectively [m^2]
$D_{i,cx}$, $D_{i,cy}$ quantities defined by equation (14) [sr]
E emissive power [W m^{-2}]
$F_{i\to j}$ generalized radiation exchange factor from zone i to zone j
G irradiation [W m^{-2}]
I radiation intensity [W m^{-2} sr^{-1}]
I_n, I_{n+1} Radiation intensities entering and leaving a control volume, respectively [W m^{-2} sr^{-1}]
i unit vector along x-direction
J radiosity [W m^{-2}]
j unit vector along y-direction
K number of volume zones
N number of surface zones
N_θ, N_φ number of polar and azimuthal solid angles per octant, respectively
n unit vector normal to the wall
q net heat flux [W m^{-2}]
Q net heat rate [W]
$\underline{S}$ source term [W m^{-3} sr^{-1}]
$\overline{S_iS_j}$ total surface-surface exchange area [m^2]
$\overline{\overline{S_iG_k}}$ total surface-volume exchange area [m^2]
s direction of a radiation beam [m]
s unit vector along direction s
T temperature [K]
V volume [m^3]
x, y coordinate directions [m]
w_j quadrature weight associated with the j-direction.

Greek symbols
γ weighted diamond differencing
δs distance travelled by a radiation beam within a control volume [m]
$\Delta\Omega$ solid angle [sr]
ε emissivity
θ polar angle
κ absorption coefficient [m^{-1}]
ξ, η direction cosines
σ Stefan–Boltzmann constant
ϕ azimuthal angle.

Subscripts
b black body
e exit from a control volume
i entrance into a control volume
P grid node
PQ_i direction defined by points P and Q_i
s surface
w wall.

to circumvent these difficulties is by modelling the panels of superheaters as obstacles of zero thickness, hereafter referred to as baffles. The simulation of enclosures with baffles presents a new situation which does not appear in case of obstacles of finite thickness, as treated in the works mentioned above. The new situation is the occurrence of adjacent control volumes, both within the physical domain, but with a solid interface which prevents radiation beams from crossing it.

The objective of this paper is to adapt radiation models, suitable for incorporation in reactive fluid flow codes, to handle enclosures with baffles and containing an emitting–absorbing medium. The following methods were selected for this purpose: the discrete transfer, the discrete ordinates and the finite volume method. In addition, the zone method is employed as a reference for comparison purposes, using the Monte-Carlo method to calculate the total exchange areas. A brief description of these methods, with an emphasis placed on the modifications required to handle the baffles, is presented below. The methods are then applied to three test cases and the results obtained are presented and discussed.

2. THE RADIATION MODELS

The radiation models are described below, with emphasis placed on the treatment of the baffles.

2.1. *The zone method (ZM)*

In the zone method the enclosure is divided into a finite number of isothermal volume and surface zones, and energy balances are performed for the radiative exchange between any two zones. The net radiative heat rate for surface zone i is calculated as:

$$Q_{si} = \sum_{j=1}^{N} \overline{S_iS_j}E_{bsj} + \sum_{k=1}^{K} \overline{\overline{S_iG_k}}E_{bgk} - \varepsilon_i A_i E_{bsi} \quad (1)$$

and a similar equation may be written for a volume zone k. The basic equations of the zone method are applied to an enclosure with baffles in the same ways as to an empty enclosure. This means that an equation is considered for each zone of the enclosure, including the surface zones on both sides of each baffle. Therefore, dealing with the baffles does not require any especial treatment within the framework of the zone method.

The total surface–surface and volume–surface exchange areas may be expressed as:

$$\overline{S_iS_j} = A_j\varepsilon_j F_{j\to i} \tag{2}$$

$$\overline{S_iG_k} = 4\kappa_k V_k F_{k\to i}. \tag{3}$$

The generalized radiation exchange factor F between surface zone j (or volume zone k) and surface zone i is defined as the fraction of the total energy emitted by surface zone j (or volume zone k) that is absorbed by surface zone i, either directly or after any number of reflections.

The radiation exchange factors were calculated using the Monte-Carlo method [5, 16, 17] and emitting 100,000 energy bundles from each surface and volume zones. The generalized radiation exchange factor between zone j and zone i is approximated as the ratio of the number of bundles absorbed by zone i and originally emitted from zone j, to the total number of bundles released from zone j. Once the coordinates of the emission point of a bundle, its direction and the distance travelled before absorption have been randomly defined, the point where the bundle intersects a boundary (wall or baffle) must be determined. When tracking an energy bundle in a geometry with baffles, it is necessary to check if the baffles are crossed or not. To simplify the calculation of the coordinates of the point where the energy bundle hits a boundary, the enclosure is divided into smaller ones, such that the small enclosures do not contain any baffle.

An example is illustrated in Fig. 1, which shows an enclosure with three baffles divided into four subdomains: A, B, C and D. An energy bundle emitted from a surface or volume zone of subdomain A may be absorbed by a surface or volume zone of that subdomain (e.g. energy bundle E_1 in Fig. 1) or may pass to the neighbouring subdomain B without being absorbed (e.g. energy bundles E_2, E_3 and E_4 in Fig. 1). To distinguish these two situations, the coordinates of the point where the energy bundle intersects the boundary of subdomain A are determined. If the energy bundle passes to subdomain B, then the coordinates of the point where it crosses again the boundary of subdomain B must be determined. Hence, it will be possible to find if the energy bundle is absorbed by a surface or volume zone in subdomain B, if it passes to subdomain A (after one or more reflections) or passes to subdomain C (e.g. energy bundles E_3 and E_4 in Fig. 1). This procedure is repeated until the energy bundle is absorbed. Energy bundles emitted from zones in other subdomains are treated similarly.

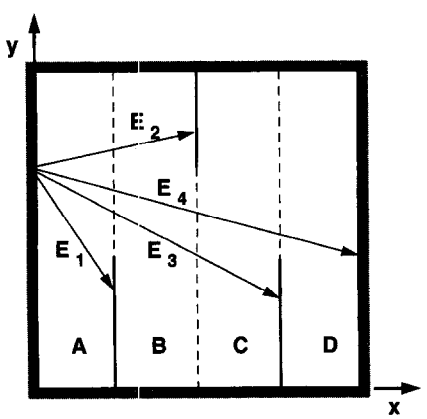

Fig. 1. Division of an enclosure into subdomains.

In this way, the problem of tracking the energy bundles in a geometry with baffles is decomposed into smaller problems, such that each one of them consists in a standard problem of tracking an energy bundle in a geometry without baffles.

2.2. *The discrete transfer method (DTM)*

The DTM is based on the solution of the radiative heat transfer equation along specified directions. If a non-scattering grey medium in local thermodynamic equilibrium is assumed, this equation may be written for a radiation beam travelling along direction s in the following form

$$\frac{\mathrm{d}I}{\mathrm{d}s} = -\kappa I + \kappa I_\mathrm{b}. \tag{4}$$

The physical domain is divided into control volumes and the temperature and absorption coefficient of the medium are taken as constant in each one of them. Then, the central point P of each cell on the boundary is determined and a hemisphere centred at P is considered and subdivided into a prescribed number of solid angles. Each solid angle defines a direction along which the radiative transfer equation is solved.

Hence, given a point P at the centre of a cell face on the boundary a radiation beam is fired from P for each one of the directions selected above. The path of a radiation beam is followed until it hits another boundary. Let Q_i be the impingement point, as shown in Fig. 2(a). Although, in general, Q_i is not the central point of a boundary cell, it is assumed that the radiation intensity at Q_i and at the central point of the cell containing Q_i are equal. Then, starting from Q_i, the path of the beam is followed back to the origin P and equation (4) is integrated analytically along this path yielding the recurrence relation

$$I_{n+1} = I_n \mathrm{e}^{-\kappa\delta s} + I_\mathrm{b}(1-\mathrm{e}^{-\kappa\delta s}). \tag{5}$$

If there are baffles, they are regarded as additional boundaries. This means that, in the example illustrated in Fig. 2(b), equation (4) would be integrated only from R to P. Radiation beams are also fired from the baffles. Hence, taking the cell face centred at point A as an example [see Fig. 2(b)], a hemisphere centred at A, on the left-hand side of the baffle, defines new directions along which equation (4) is solved, e.g. direction $\overrightarrow{AB}$. Similarly, the hemisphere centred at A, on the right-hand side of the baffle, determines new directions, such as $\overrightarrow{AC}$.

The incident radiative heat fluxes G at the central

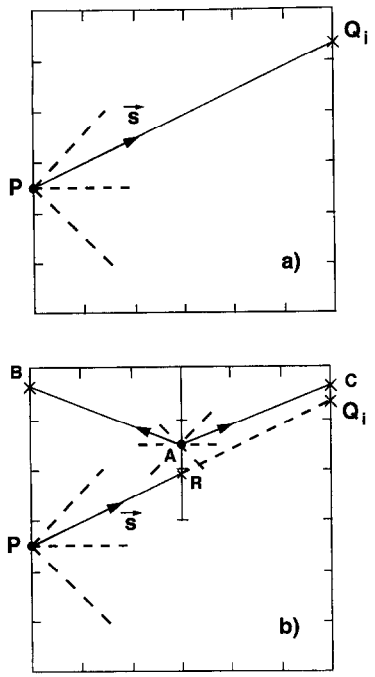

Fig. 2. Ray tracing in the discrete transfer method.

points of cell faces on the boundary (e.g. point P), or at the central points of cell faces on the baffles (e.g. point A), are calculated by adding up the contributions due to all the radiation beams that reach those points. Thus, the incident heat flux at P is given by

$$G_P = \sum_i I_{PQ_i}(\mathbf{s}_{PQ_i} \cdot \mathbf{n}) \Delta\Omega_{PQ_i} \tag{6}$$

where the summation extends over all the directions associated to the solid angles resultant from the discretization of the hemisphere centred at P. In this equation, $\mathbf{n}$ is the unit vector normal to the wall at point P, and $\mathbf{s}$ is the unit vector along the direction from P to Q_i. This direction is denoted by the subscript PQ_i.

The solution of the radiative heat transfer equation requires as boundary conditions knowledge of the temperature or heat flux distribution along the wall and on both sides of the baffles. The two sides of a baffle may have different emissivities and temperatures. If the wall temperature is prescribed, the boundary condition may be written as:

$$J_P = \varepsilon_w \sigma T_w^4 + (1-\varepsilon_w) G_P. \tag{7}$$

Other boundary conditions are dealt with as reported in [6]. The calculation procedure is iterative, unless $\varepsilon_w = 1$, because the radiation intensities at the boundaries are not known *a priori*.

2.3. *The discrete ordinates method (DOM)*

The DOM relies on a discrete representation of the directional dependence of the radiation intensity. The radiative heat transfer equation (4) is solved for a set of directions which span the total solid angle range of 4π around a point in space, and the integrals over solid angles are approximated using a numerical quadrature rule. The direction cosines and the quadrature weights used in the present work were taken from Modest [5].

Equation (4) may be written as follows for any discrete direction $\mathbf{s}_i$ and for a two-dimensional problem:

$$\xi_i \frac{\partial I_i}{\partial x} + \eta_i \frac{\partial I_i}{\partial y} = -\kappa I_i + \kappa I_b + S. \tag{8}$$

S is a source term used to deal with the baffles, identical to the one proposed by Chai *et al.* [14] to deal with irregular geometries using Cartesian coordinates. The source term is zero, except for the control volumes adjacent to the boundaries (walls or baffles), and it is used to insert the boundary conditions as explained below.

Equation (8) is integrated over each control volume, yielding a relationship between the volume average intensity, I_{P_i}, and the radiation intensities entering (subscript i) and leaving subscript e) the control volume [14]:

$$I_{P_i} = \frac{(\kappa I_b + S) V\gamma + |\xi_i| A_x I_{x_i,i} + |\eta_i| A_y I_{y_i,i}}{\kappa V\gamma + |\xi_i| A_x + |\eta_i| A_y}. \tag{9}$$

The parameter γ relates the incoming and outgoing radiation intensities to the volume average intensity, according to the following relations:

$$I_{P_i} = \gamma I_{x_e,i} + (1-\gamma) I_{x_i,i} \tag{10a}$$

$$I_{P_i} = \gamma I_{y_e,i} + (1-\gamma) I_{y_i,i}. \tag{10b}$$

The most commonly used values of γ are $\gamma = 1/2$ (diamond scheme) and $\gamma = 1$ (step scheme). The step scheme was used in the present work.

The boundary conditions may be written as follows, taking as an example a surface with x = constant and $\xi_i > 0$:

$$I_i = \varepsilon_w I_{bw} + \frac{1-\varepsilon_w}{\pi} \sum_{\xi_j < 0} w_j I_j |\xi_j|. \tag{11}$$

This boundary condition is also valid for the right-hand side of a vertical baffle. It is enforced via the source term S by setting

$$S = \frac{|\xi_i| A_x}{V\gamma} \left(\varepsilon_w I_{bw} + \frac{1-\varepsilon_w}{\pi} \sum_{\xi_j < 0} w_j I_j |\xi_j| \right) \tag{12}$$

for the control volumes adjacent to the boundary, and by putting $I_{x_i,i} = 0$ in equation (9). The remaining boundaries (x = constant and $\xi_i < 0$; y = constant and $\eta_i > 0$; y = constant and $\eta_i < 0$) are treated similarly.

The numerical solution of equation (9) is carried out starting from one of the corners of the computational domain, depending on the sign of the direc-

tion cosines. In each iteration, and for each one of the selected directions, the radiosity of the boundaries and the internal radiation sources in each cell are either known or guessed from the values computed in the previous iteration. Hence, all the control volumes are visited to compute the radiation intensities I_{P_i} according to (9) and using the auxiliary relations (10). After all the directions have been treated, the radiosities of the boundaries and the radiation sources may be updated and the iteration process continues until the convergence criterion has been satisfied.

2.4. *The finite volume method (FVM)*

The FVM has many similarities with the DOM. The magnitude of the radiation intensity is also assumed constant in each discrete direction, and the radiative transfer equation is solved for a set of discrete directions which span the total solid angle of 4π.

To obtain the discrete equations, the radiative transfer equation is integrated over each control volume and each solid angle in which the space is discretized. While in the DOM the direction $\mathbf{s}_i$ is taken as a constant within the solid angle $\Delta\Omega_i$, in the FVM it varies, following the variation of the polar and azimuthal angles within $\Delta\Omega_i$. Therefore, a different discretized equation is obtained, which may be written as follows [15]:

$$I_{P_i} = \frac{(\kappa I_b + S) V\gamma\Delta\Omega_i + D_{i,cx}A_x I_{x,i} + D_{i,cy}A_y I_{y,i}}{\kappa V\gamma\Delta\Omega_i + D_{i,cx}A_x + D_{i,cy}A_y} \tag{13}$$

where

$$D_{i,cx} = \int_{\Delta\Omega_i} \mathbf{s}_i \cdot \mathbf{i}\, d\Omega_i,\ D_{i,cy} = \int_{\Delta\Omega_i} \mathbf{s}_i \cdot \mathbf{j}\, d\Omega_i \tag{14}$$

and

$$\Delta\Omega_i = \int_{\Delta\phi_i}\int_{\Delta\theta_i} \sin\theta\, d\theta\, d\phi. \tag{15}$$

The source term S has the same meaning and plays the same role explained above for the DOM. The discrete ordinates equation (9) would be recovered from equation (13) by replacing $D_{i,cx}$ and $D_{i,cy}$ by $|\xi_i|$ and $|\eta_i|$, respectively, and by deleting $\Delta\Omega_i$ from the numerator and denominator.

The boundary conditions may be written as follows for a surface with x = constant and $D_{i,cx} > 0$:

$$I_i = \varepsilon_w I_{bw} + \frac{1-\varepsilon_w}{\pi} \sum_{\mathbf{s}_j\cdot\mathbf{n}<0} I_j \int_{\Delta\Omega_j} |\mathbf{S}_j \cdot \mathbf{i}|\, d\Omega_j. \tag{16}$$

This boundary condition is introduced by evaluating the source term S as:

$$S = \frac{D_{i,cx}A_x}{V\gamma\Delta\Omega_i}\left(\varepsilon_w I_{bw} + \frac{1-\varepsilon_w}{\pi} \sum_{\mathbf{s}_j\cdot\mathbf{n}<0} I_j \int_{\Delta\Omega_j} |\mathbf{S}_j \cdot \mathbf{i}|\, d\Omega_j\right) \tag{17}$$

for the control volume adjacent to the boundary (wall or baffle) and by setting $I_{x,i} = 0$ in equation (13). A similar treatment is used for the other boundaries. The solution procedure is identical to that described for the DOM.

3. RESULTS AND DISCUSSION

The radiation models described above were applied to three test cases. The results obtained are presented and discussed in this section.

3.1. *Two-dimensional square enclosure with one baffle*

A two-dimensional square enclosure was considered in the first test case. A baffle is suspended on the top wall, as shown in Fig. 3. This figure also shows an auxiliary coordinate s used to present the results, which runs along the wall and along the baffle. The enclosure contains a grey medium with an emissive power equal to 10 W m^{-2}. Calculations were performed for two different boundary conditions. In the first case the boundaries, including the baffle, are assumed black, and in the second case the emissivity of the walls in 0.8 and the emissivity of the baffle is 0.6. In both cases, a unity emissive power is considered for the walls and for the baffle.

To check the correctness of the treatment of the baffles, preliminary calculations were performed simulating the whole enclosure depicted in Fig. 3, as well as only one half of the enclosure. In this case, a symmetry boundary condition was prescribed at $x = 0.5$ m, from $y = 0$–0.6 m. These results are not presented here, but it was verified that the net heat flux along the boundary, including the surface of the baffle, are identical in the two cases, demonstrating the correct implementation of the baffle treatment.

Figure 4 shows the predicted evolution of the net heat flux along the boundary for a black enclosure containing a medium with an absorption coefficient

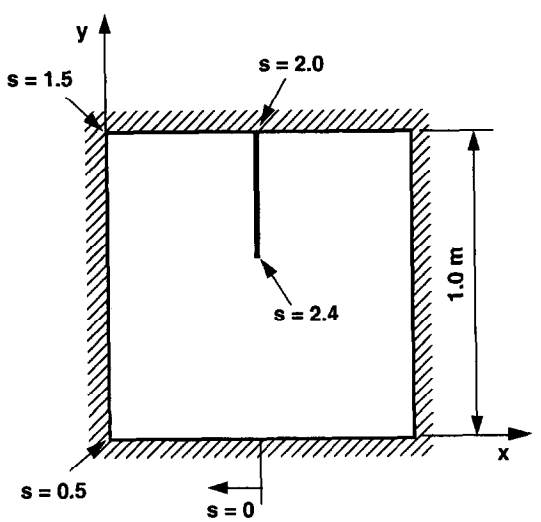

Fig. 3. Geometry of the enclosure studied in test case 1.

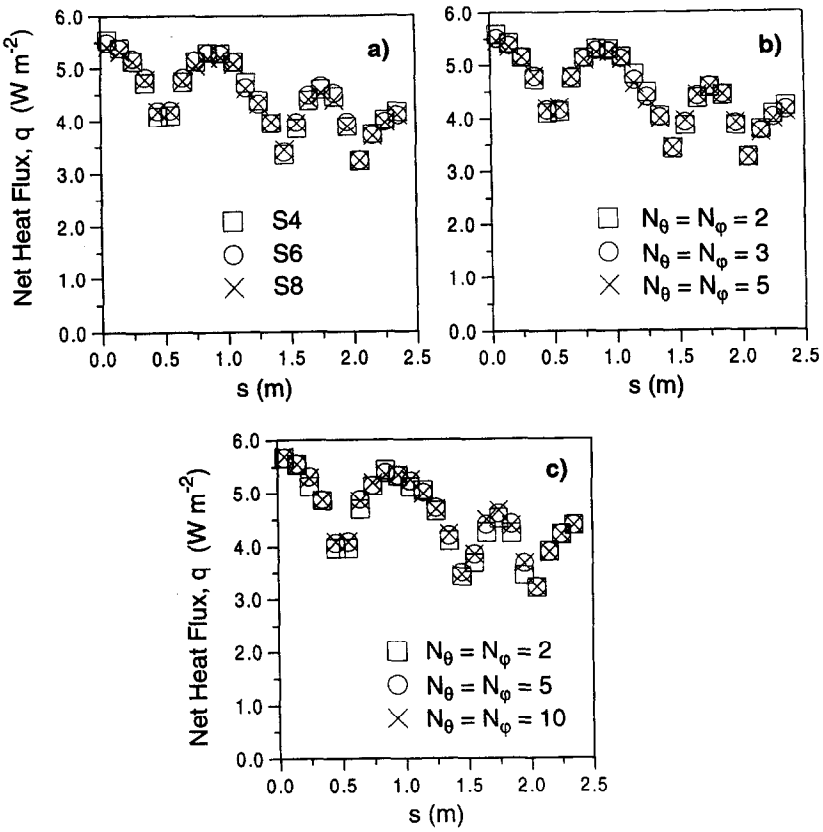

Fig. 4. Predicted net heat flux (W m^{-2}) along the boundary of a square black enclosure with one baffle containing an emitting-absorbing medium with $\kappa = 1\ m^{-1}$: (a) discrete ordinates method; (b) finite volume method; (c) discrete transfer method.

equal to 1 m^{-1}. A uniform grid with 10×10 control volumes was used, and the results of several angular discretizations are shown. The S4, S6 and S8 approximations were used in the DOM, 2×2, 3×3 and 5×5 ($N_\theta \times N_\varphi$) angles per octant were employed in the FVM and 2×2, 5×5 and 10×10 directions per octant were considered in the DTM. The results show relatively small differences for the angular discretizations selected in the DOM and FVM, larger differences between the different discretizations being 2.5 and 2.0%, respectively. In the DTM the two finer angular discretizations yield similar results, but the coarser one departs from them, with larger differences of about 6.7%.

Figure 5 shows a comparison of the results obtained for the same problem, and the same methods, but using a finer grid (20×20 control volumes) and finer angular discretizations. The results of the zone method calculated using 10×10 uniform volume zones are also plotted, both with and without the baffle. The net heat fluxes are larger at the centre of the walls and decrease towards the corners. It can be seen that the presence of the baffle has a minor influence on the heat flux along the bottom wall ($0 \leqslant s \leqslant 0.5$ m). However, the influence of the baffle becomes more important along the west wall, as s increases up to 1.5 m, and especially on the top wall ($1.5 \leqslant s \leqslant 2.0$ m), close to the baffle. Since the emissive power of the baffle surface is small compared to the emissive power of the medium, the presence of the

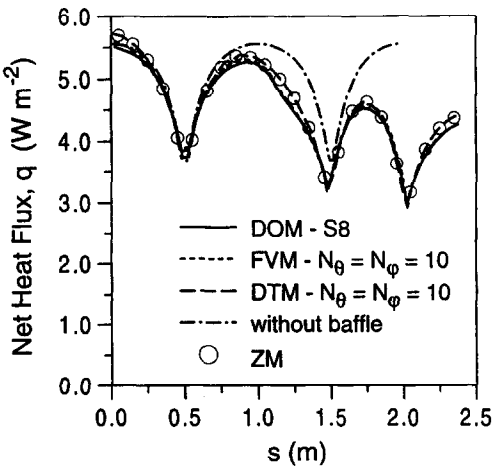

Fig. 5. Predicted net heat flux (W m^{-2}) along the boundary of a square black enclosure with one baffle containing an emitting-absorbing medium with $\kappa = 1\ m^{-1}$.

baffle causes a decrease of the net heat flux along the boundary. The numerical solutions computed using the four different methods are very close to each other. In particular, the DTM and ZM solutions are almost coincident, while the DOM and FVM solutions yield slightly lower net heat fluxes close to the centre of the walls, and on the tip of the baffle.

Additional calculations were performed for other values of the absorption coefficient ($\kappa = 0.1$ and 10 m^{-1}), and repeated for the case of grey boundaries. A grid with 10×10 control volumes was used in all the cases. The S4 approximation was employed in the DOM, and the same number of discrete solid angles (24) was taken in the FVM ($N_\theta = 1$, $N_\varphi = 3$), while a slightly larger number of directions (32) was used in the DTM ($N_\theta = 2$, $N_\varphi = 2$). The results are presented in Fig. 6.

Figure 6 shows that the net heat fluxes increase with the absorption coefficient of the medium. The flux distribution along the walls is more uniform for larger κ, but exhibits a sharper drop close to the corners. The influence of the baffle is progressively attenuated with the increase of the absorption coefficient. In the case of grey boundaries, the net heat fluxes are smaller than for black boundaries, especially when the absorption coefficient of the medium is high. Moreover, for

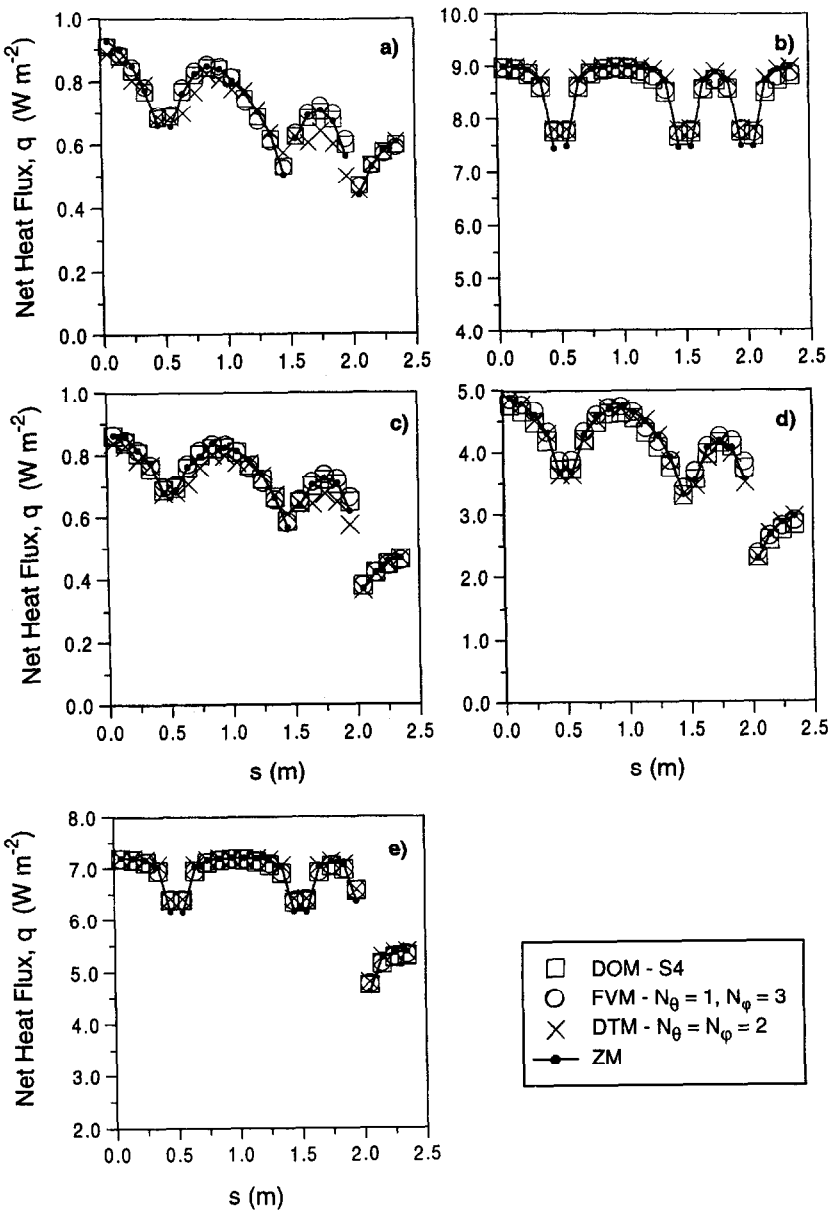

Fig. 6. Predicted net heat flux (W m^{-2}) along the boundary of a square enclosure with one baffle: (a) black boundaries, $\kappa = 0.1$ m^{-1}; (b) black boundaries, $\kappa = 10$ m^{-1}; (c) grey boundaries, $\kappa = 0.1$ m^{-1}; (d) grey boundaries, $\kappa = 1$ m^{-1}; (e) grey boundaries, $\kappa = 10$ m^{-1}.

grey boundaries a fast variation of the net heat flux occurs close to $s = 2$ m, as a consequence of the different emissivities of the wall and surface of the baffle.

A comparison of the numerical solutions obtained by the different methods shows that they all predict similar evolutions of the net heat fluxes. If the absorption coefficient of the medium is small ($\kappa = 0.1$ m^{-1}), the DTM generally yields the lowest heat fluxes, both for black and grey boundaries, especially on the top wall of the enclosure. The results of the remaining three methods are close to each other. In the case of an absorption coefficient equal to 1 or 10 m^{-1}, the differences between the solutions of the several methods are small. It is worth noting, however, that for the higher absorption coefficient the DOM, FVM and DTM predictions do not drop as sharply as the ZM results close to the corners of the enclosure.

Although there is a good agreement between the numerical solutions of the different methods, the computational requirements are not the same. The CPU time required to obtain the converged solution is similar for the DOM and the FVM. The DTM has required about five times more CPU time for identical spatial and angular discretizations. The ZM is by far the most expensive method. The calculations for the 10×10 uniform grid using the zone method require eight times more CPU time than corresponding calculations using the DOM, an 80×80 uniform grid and the S8 approximation.

3.2. *Two-dimensional square enclosure with three baffles*

A two-dimensional square enclosure was also investigated in the second test case, but two additional baffles were introduced, as shown in Fig. 7. The emissive power and the absorption coefficient of the medium are 10 W m^{-2} and 0.1 m^{-1}, respectively. The boundary conditions are the same considered in the previous test case.

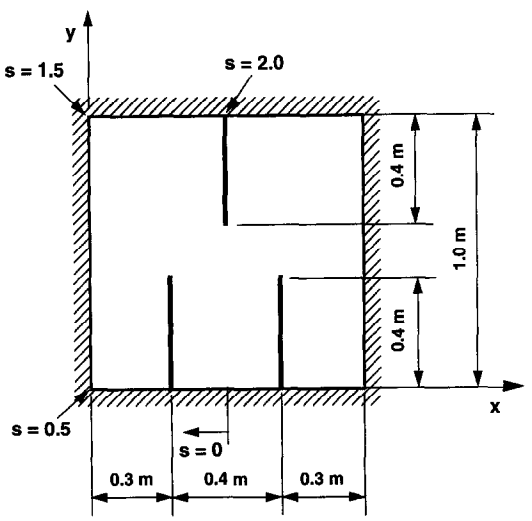

Fig. 7. Geometry of the enclosure studied in test case 2.

A grid with 10×10 volume zones was employed in the zone method calculations, while 40×40 control volumes were used in the DOM, FVM and DTM. The S8 approximation was used in the DOM, and 10×10 angles per octant were used both in the FVM and DTM. The predicted net heat fluxes along the boundary are plotted in Fig. 8. The coordinate s runs along the wall, from the centre of the bottom wall up to the centre of the top wall, as depicted in Fig. 7. The coordinate z is measured along the baffles, from the wall to the tip of the baffles.

The introduction of the two baffles attached to the bottom wall, comparatively to test case 1, causes a decrease of the net heat fluxes, especially along the bottom wall. Those two baffles divide the bottom wall into three regions, and the net heat fluxes exhibit a similar distribution in each region, achieving a maximum at the centre and decreasing towards the edges. The heat fluxes distribution is similar for black and grey boundaries.

All the methods yield similar predictions, although the peak of the heat fluxes calculated by the DOM is smaller than that computed by the other methods at the bottom ($s = 0$ m) and the top walls ($s = 1.75$ m). Moreover, the predicted evolution along the west wall ($0.5 \leqslant s \leqslant 1.5$ m) is not as smooth as the distributions computed using the FVM, DTM and ZM. This suggests that the S8 approximation may be responsible for the observed behaviour, since it corresponds to a coarser angular discretization than that used in the FVM and DTM. The computational requirements of the different methods are similar to those observed in the previous test case. The only difference is that the DTM converges in a smaller number of iterations than the DOM and the FVM. However, an iteration of the DTM takes more time and, overall, it has required 2.5 times more CPU time to converge than the DOM and the FVM.

3.3. *Three-dimensional enclosure*

In the last test case a three-dimensional enclosure resembling the combustion chamber of a utility boiler was modelled. The enclosure contains five baffles, as shown in Fig. 9, which simulate the panels of superheaters that may be suspended from the top of the combustion chamber. The temperature and the emissivity of the boundaries, including the surface of the baffles, were taken as 800 K and 0.65, respectively, except at $x = 10$ m and for $22 \leqslant z \leqslant 30$ m, where the temperature was set equal to 1200 K and a black body surface was assumed. An emitting–absorbing medium was assumed, with the following distributions of temperature and absorption coefficient:

$$\text{for } z \leqslant 5 \text{ m}: \kappa = 0.20 \text{ m}^{-1}, T = 1600 \text{ K}$$

$$\text{for } 5 < z \leqslant 10 \text{ m}: \kappa = 0.25 \text{ m}^{-1}, T = 2000 \text{ K}$$

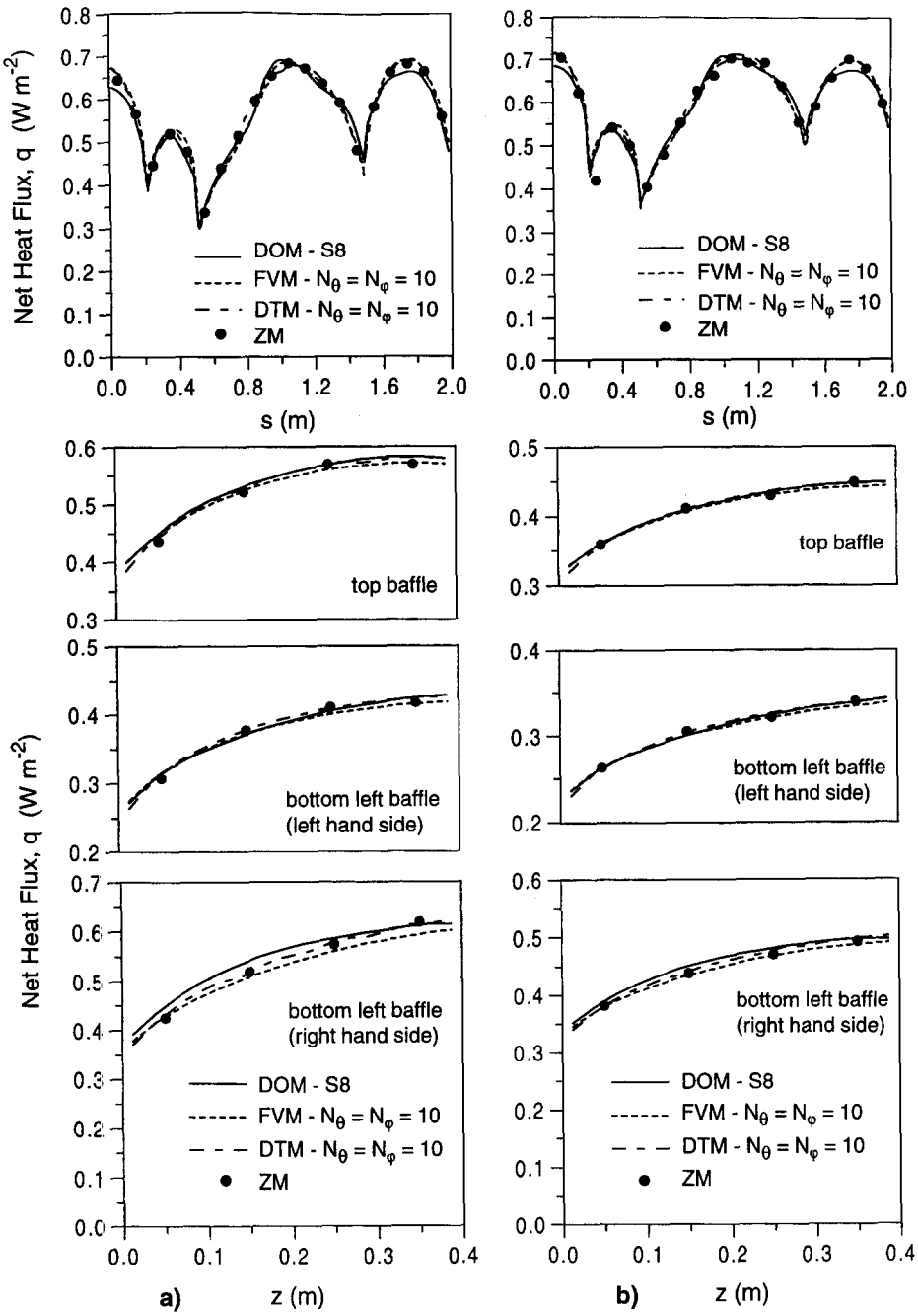

Fig. 8. Predicted net heat flux (W m^{-2}) along the boundary of a square enclosure with three baffles containing an emitting–absorbing medium with $\kappa = 0.1\ m^{-1}$: (a) black boundaries; (b) grey boundaries.

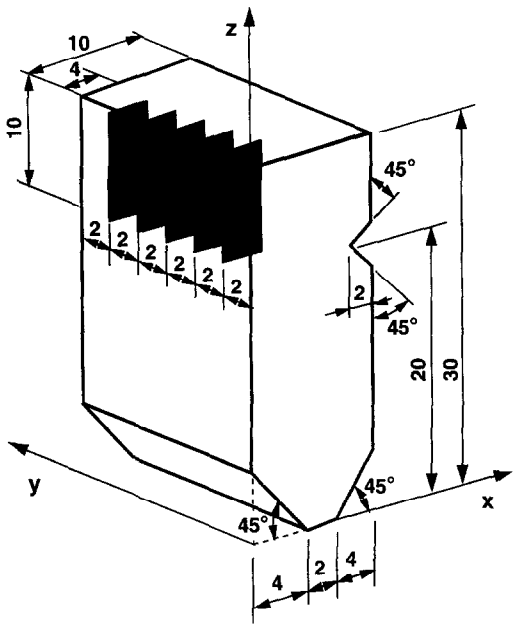

Fig. 9. Schematic of the enclosure studied in test case 3.

for $10 < z \leqslant 20$ m : $\kappa = 0.20\ \text{m}^{-1}$, $T = 1600$ K

for $20 < z \leqslant 30$ m : $\kappa = 0.18\ \text{m}^{-1}$, $T = 1200$ K.

The calculations were performed using a grid with $20 \times 60 \times 60$ control volumes, and the inclined walls were simulated in a stepwise fashion. An angular discretization with $N_\theta = N_\varphi = 5$ was employed both in the FVM and DTM calculations, while the S8 approximation was used in the DOM. We only present here the results for these three methods. In fact, the code for the calculation of the radiation exchange factors has been written only for two-dimensional enclosures with obstacles, although there are not any theoretical difficulties in the extension to three-dimensional problems.

The predicted net heat flux contours for the front, side and back walls are shown in Fig. 10. The maximum heat fluxes occur at the level where the temperature and absorption coefficient of the medium are higher, i.e. at the burners level of an actual boiler, and decrease progressively towards the top, the bottom and the vertical edges. The contour of 100 kW m^{-2} on the front wall exhibits a wavy shape due to the influence of the baffles. The local heat fluxes are larger in vertical planes equidistant from the baffles, and decrease towards the baffles, as also observed in the previous test cases. The contours are almost identical regardless of the radiation model. However, it may be seen that the contours obtained using the DTM are not as smooth as the others, particularly the contour of 100 kW m^{-2} on the front and back walls. This is not surprising since it has been observed that the DTM sometimes produces oscillatory solutions [11]. In this problem the DTM has also required less iterations, but about 1.5 times more CPU time to attain convergence than the DOM and the FVM.

4. CONCLUDING REMARKS

Four radiation models: the zone method, the discrete transfer, the discrete ordinates, and the finite volume method, were applied to the calculation of the heat fluxes in two-dimensional enclosures containing baffles, i.e. obstacles of zero thickness. Three of the models were further applied to the combustion chamber of an idealized utility boiler with several baffles. The modifications required to deal with the baffles were described.

All the methods predict similar evolutions of the net heat flux along the boundaries, both for black and grey boundaries. The predicted influence of the baffles on the distribution of the heat fluxes exhibits the expected trends. As far as the computational requirements are concerned, the discrete ordinates and the finite volume method converge faster than the discrete transfer method, by a factor which has changed between 1.5 and 5, depending on the test cases. The discrete transfer method may converge in a smaller number of iterations, but each iteration requires more CPU time. The zone method is by far the most computational demanding method.

Acknowledgements—Part of this work was financially supported by the Commission of the European Communities under the ESPRIT project 8114, HP-PIPES—"High Performance Parallel Computing for Process Engineering Simulation".

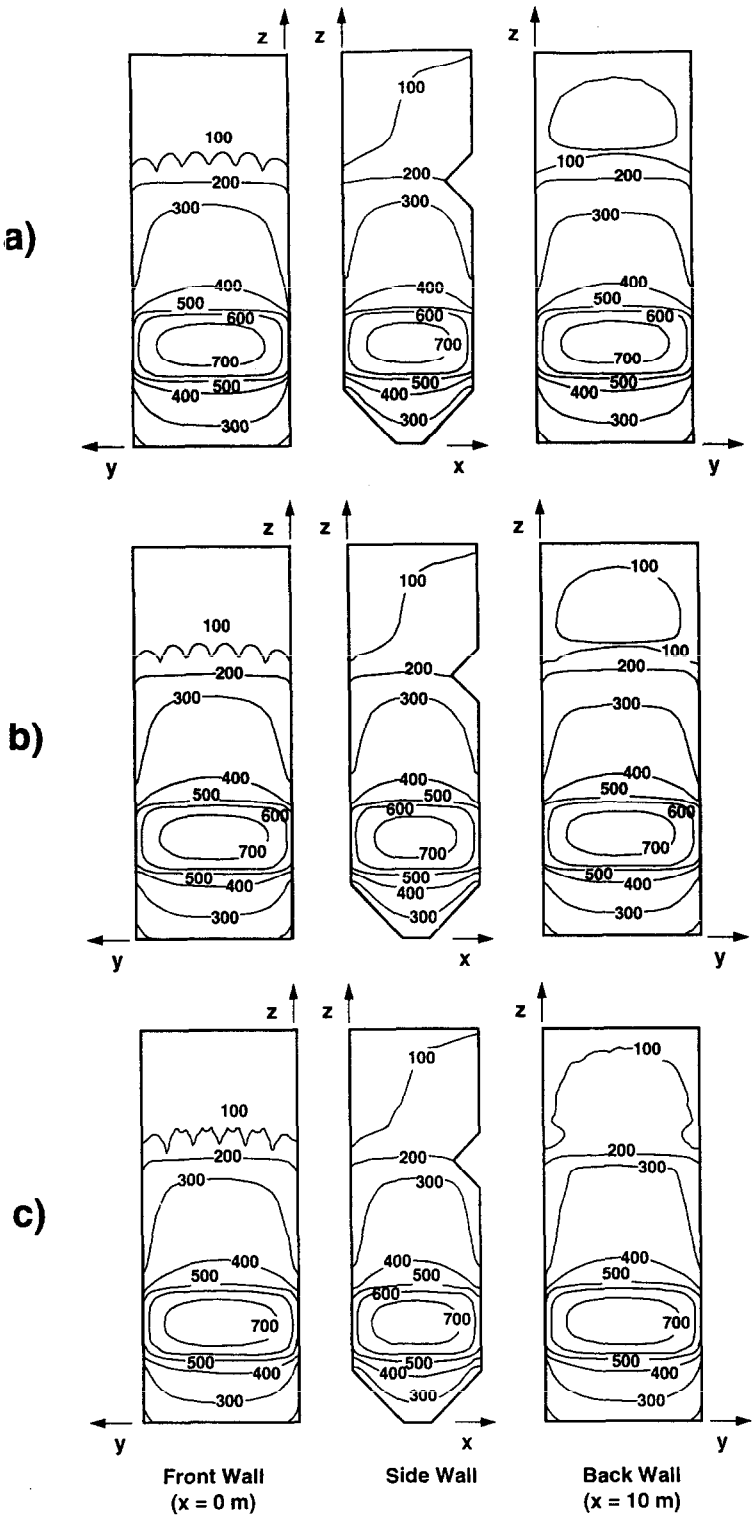

Fig. 10. Predicted net heat flux (kW m^{-2}) contours on the walls of the boiler: (a) DOM; (b) FVM; (c) DTM.

REFERENCES

1. Viskanta, R. and Menguç, M. P., Radiation heat transfer in combustion systems. *Progress in Energy and Combustion Science*, 1987, **13,** 97–160.
2. Hottel, H. C. and Sarofim, A. F., *Radiative Transfer*. McGraw-Hill, New York, 1967.
3. Howell, J. R., Application of Monte-Carlo to heat transfer problems. In *Advances in Heat Transfer*, ed. J. P. Hartnett and T. F. Irvine, Vol. 15. Academic Press, New York, 1968.
4. Selçuk, N., Evaluation of multi-dimensional flux models for radiative transfer in combustion chambers: a review, AGARD CP-353, paper 28, 1983.
5. Modest, M. F., *Radiative Heat Transfer*, McGraw-Hill, New York, 1993.
6. Lockwood, F. C. and Shah, N. G., A new radiation solution for incorporation in general combustion prediction procedures. *18th Symposium (International) on Combustion*, The Combustion Institute, 1981, pp. 1405–1414.
7. Carlson, B. G. and Lathrop, K. D., Transport theory—the method of discrete ordinates. In *Computing Methods in Reactor Physics*. Gordon and Breach, New York, 1968.
8. Fiveland, W. A., Discrete-ordinates solutions of the radiative transport equation for rectangular enclosures. *Journal of Heat Transfer*, 1984, **106,** 699–706.
9. Raithby, G. D. and Chui, E. H., A finite-volume method for predicting radiant heat transfer in enclosures with participating media. *Journal of Heat Transfer*, 1990, **112,** 415–423.
10. Chai, J. C., Lee, H. S. and Patankar, S. V., Finite volume method for radiation heat transfer. *Journal of Thermophysics and Heat Transfer*, 1994, **18,** 419–425.
11. Coelho, P. J., Gonçalves, J. M. and Carvalho, M. G., A comparative study of radiation models for coupled fluid flow/heat transfer problems. In *Numerical Method in Thermal Problems*, ed. R. Lewis and P. Durbetaki, Vol. 9, Part 1, 1995, pp. 378–389.
12. Sànchez, A. and Smith, T. F., Surface radiation exchange for two-dimensional rectangular enclosures using the discrete-ordinates method. *Journal of Heat Transfer*, 1992, **114,** 465–472.
13. Adams, B. R. and Smith P. J., Three-dimensional discrete-ordinates modeling of radiative transfer in a geometrically complex furnace. *Combustion Science and Technology*, 1993, **88,** 293–308.
14. Chai, J. C., Lee, H. S. and Patankar, S. V., Treatment of irregular geometries using a cartesian-coordinates-based discrete-ordinates method. *Radiative Heat Transfer: Theory and Applications*, 1993, **244,** 49–54.
15. Chai, J. C., Lee, H. S. and Patankar, S. V., Treatment of irregular geometries using a cartesian-coordinates finite-volume radiation heat transfer procedure. *Numerical Heat Transfer, Part B*, 1994, **26,** 225–235.
16. Trivic, D. N., Mathematical modelling of three-dimensional turbulent flow with combustion and radiation. Ph. D. thesis, University of New Brunswick, Fredericton, N. B., Canada, 1987.
17. Steward, F. R. and Trivic, D. N., An assessment of particle radiation in a pulverized-coal-fired boiler. *Journal of the Institute of Energy*, 1989, **LXII,** 138–146.